# High-pressure transitions of trigonal $\alpha$-$ZrMo_2O_8$

Stefan Carlson
*European Synchrotron Radiation Facility (ESRF), BP 220, F-38043 Grenoble Cedex, France*

Anne Marie Krogh Andersen
*Department of Chemistry, Odense University, DK-5230 Odense M, Denmark*

(Received 18 October 1999)

High-pressure synchrotron x-ray powder-diffraction studies show that trigonal $\alpha$-$ZrMo_2O_8$ transforms to a monoclinic symmetry phase ($\delta$-$ZrMo_2O_8$) at 1.06–1.11 GPa. The space group was determined to $C2/m$. A further high-pressure transition from the monoclinic $\delta$ to a triclinic $\epsilon$ phase occur at 2.0–2.5 GPa (space group $P1$ or $P\bar{1}$). Both transformations are reversible. The volume compressibilities are similar for the $\alpha$ and $\delta$ phase, and five times lower for the $\epsilon$ phase.

This study was performed as part of high-pressure investigations on $MX_2O_8$ and $MX_2O_7$ compounds ($M$=Zr, Ti, Hf and $X$=P, V, Mo, W). The interest in these types of compounds during the last years is mainly due to the isotropic negative thermal-expansion properties of, e.g., $ZrW_2O_8$,[1] $HfW_2O_8$,[2] $ZrV_2O_7$,[3] and cubic $ZrMo_2O_8$.[4] Several different polymorphs of $ZrMo_2O_8$ have previously been reported in the literature: cubic[4] (hereafter $\gamma$-$ZrMo_2O_8$), trigonal[5,6] (hereafter $\alpha$-$ZrMo_2O_8$), and monoclinic[7–9] (hereafter $\beta$-$ZrMo_2O_8$). The structure of $\alpha$-$ZrMo_2O_8$ was solved from single-crystal data by Auray *et al.*[5] and Serezhkin *et al.*[6] The structure has the space-group symmetry $P\bar{3}c$ with unit-cell parameters, $a=10.1391(6)$, $c=11.7084(8)$ Å and $V=1042.2(2)$ Å$^3$. It is a two-dimensional network with layers perpendicular to the $c$ axis. The layers are built from $ZrO_6$ octahedra linked together by $MoO_4$ tetrahedra. Each

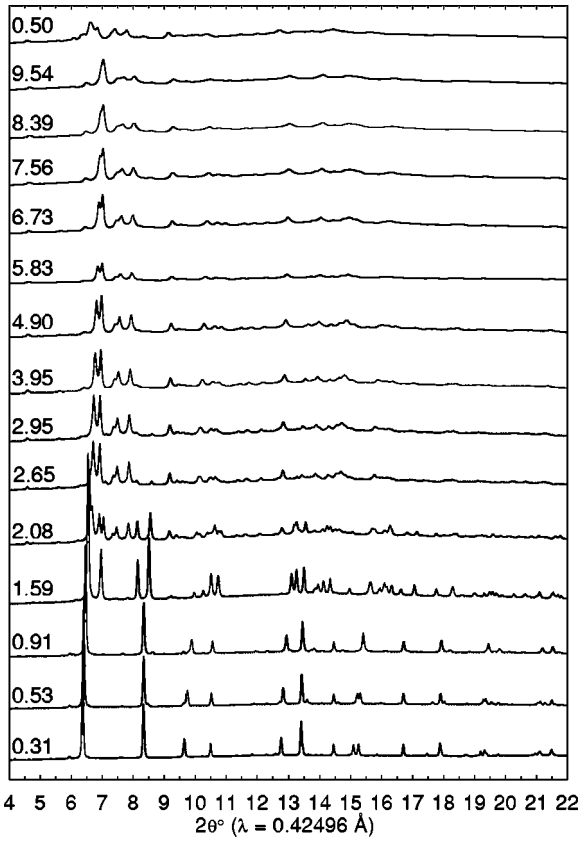


FIG. 1. The high-pressure transformations of $\alpha$-$ZrMo_2O_8$ up to 9.54 GPa. Pressures are given on the left in gigapascal. The top diagram is collected at decreasing pressure. Sample-detector distance was 450 mm.

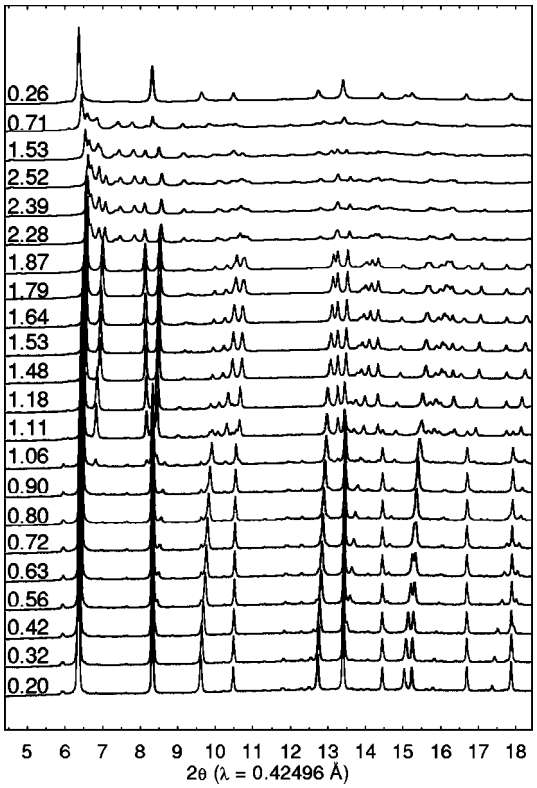


FIG. 2. The high-pressure transformations of $\alpha$-$ZrMo_2O_8$ up to 2.52 GPa. Pressures are given on the left in gigapascal. The three top diagrams are collected at decreasing pressures. Sample-detector distance was 500 mm.

 

TABLE I. The high-pressure unit-cell dimensions of $\alpha$-, $\delta$- and $\epsilon$- $ZrMo_2O_8$. Estimated standard deviations are given in parenthesis.

| $P$ (GPa) | $a$ (Å) | $b$ (Å) | $c$ (Å) | $\alpha$ (°) | $\beta$ (°) | $\gamma$ (°) | $V$ (Å$^3$) |
|---|---|---|---|---|---|---|---|
| 0.20(3) | 10.0973(2) | | 11.6583(2) | | | | 1029.37(2) |
| 0.26(3)[a] | 10.1035(6) | | 11.5942(11) | | | | 1025.00(15) |
| 0.32(3) | 10.0911(1) | | 11.6092(3) | | | | 1023.80(2) |
| 0.42(3) | 10.0964(1) | | 11.5576(3) | | | | 1020.32(3) |
| 0.56(3) | 10.0876(1) | | 11.4710(2) | | | | 1010.90(2) |
| 0.63(3) | 10.1002(1) | | 11.4416(3) | | | | 1010.83(4) |
| 0.71(3)[a] | 10.0918(7) | | 11.3335(16) | | | | 999.61(11) |
| 0.71(3)[a] | 9.846(3) | 6.080(2) | 5.3239(14) | | 92.39(3) | | 318.45(14) |
| 0.72(3) | 10.0944(2) | | 11.3895(4) | | | | 1005.06(5) |
| 0.80(3) | 10.0893(1) | | 11.3378(3) | | | | 999.49(4) |
| 0.90(3) | 10.0845(1) | | 11.2771(4) | | | | 993.20(4) |
| 1.06(3) | 10.0889(4) | | 11.2184(8) | | | | 988.90(10) |
| 1.11(3) | 10.1766(5) | | 10.9268(8) | | | | 980.01(9) |
| 1.11(3) | 9.9551(3) | 5.9974(2) | 5.4404(2) | | 92.768(3) | | 324.44(1) |
| 1.18(3) | 9.8414(3) | 5.9454(2) | 5.3663(2) | | 92.815(3) | | 313.61(1) |
| 1.48(4) | 9.7943(3) | 5.9601(2) | 5.3010(2) | | 93.002(2) | | 309.02(2) |
| 1.53(4) | 9.7741(3) | 5.9564(2) | 5.2793(2) | | 93.051(3) | | 306.92(2) |
| 1.53(4)[a] | 9.7616(8) | 5.9684(6) | 5.3299(7) | | 91.936(11) | | 310.35(4) |
| 1.53(4)[a] | 5.4202(6) | 10.320(2) | 5.1251(9) | 97.697(10) | 93.628(5) | 101.452(11) | 277.25(6) |
| 1.64(4) | 9.7568(3) | 5.9581(1) | 5.2586(2) | | 93.081(3) | | 305.25(1) |
| 1.79(4) | 9.7383(4) | 5.9657(2) | 5.2412(3) | | 93.113(3) | | 304.06(2) |
| 1.87(4) | 9.7219(3) | 5.9652(2) | 5.2268(2) | | 93.139(3) | | 302.67(2) |
| 2.28(4) | 9.6762(5) | 5.9767(3) | 5.1649(4) | | 93.090(5) | | 298.26(3) |
| 2.28(4) | 5.4377(7) | 10.2325(13) | 5.1264(8) | 94.964(12) | 93.560(7) | 103.051(12) | 275.85(7) |
| 2.39(4) | 9.6530(6) | 5.9722(4) | 5.1490(5) | | 93.100(6) | | 296.40(4) |
| 2.39(4) | 5.4299(7) | 10.2242(10) | 5.1188(5) | 94.962(9) | 93.553(8) | 103.082(9) | 274.79(5) |
| 2.52(4) | 9.6383(10) | 5.9701(7) | 5.1357(7) | | 93.139(7) | | 295.07(6) |
| 2.52(4) | 5.4311(8) | 10.2164(10) | 5.1160(6) | 94.977(10) | 93.589(10) | 103.107(9) | 174.44(5) |
| 2.65(5) | 5.4268(7) | 10.255(2) | 5.1234(6) | 97.155(12) | 93.394(9) | 101.450(13) | 276.25(8) |
| 2.95(5) | 5.4175(11) | 10.187(3) | 5.1126(9) | 97.129(15) | 93.315(16) | 101.503(16) | 273.35(11) |
| 3.95(7) | 5.4034(7) | 10.1882(17) | 5.0802(6) | 97.285(12) | 93.216(11) | 101.191(12) | 271.20(7) |
| 4.90(8) | 5.3851(7) | 10.1389(17) | 5.0558(6) | 97.313(12) | 93.121(12) | 101.050(11) | 267.84(7) |
| 5.83(9) | 5.3551(6) | 10.0626(11) | 5.0263(5) | 97.487(8) | 92.682(7) | 100.421(8) | 263.42(5) |
| 6.73(10) | 5.3516(7) | 10.0290(15) | 5.0037(6) | 97.584(10) | 92.897(12) | 100.431(10) | 261.04(6) |
| 7.56(12) | 5.3412(7) | 10.0103(15) | 4.9828(6) | 97.687(10) | 92.806(12) | 100.068(9) | 259.24(6) |
| 8.39(14) | 5.3286(8) | 10.0008(17) | 4.9615(7) | 97.767(11) | 92.748(14) | 99.748(11) | 257.51(7) |
| 9.54(15) | 5.3011(12) | 9.980(2) | 4.9201(12) | 97.856(14) | 92.545(19) | 99.423(14) | 253.77(10) |

[a]Decreasing pressures.

tetrahedral molybdate group is linked via three of the oxygen atoms to three different zirconium atoms. The fourth oxygen in the $MoO_4$ tetrahedron points into the interlayer region. The oxygen atoms form a cubic close-packed anion arrangement in the structure.

Comprehensive studies on the high-pressure properties of $ZrW_2O_8$ have previously been performed,[10–12] showing a transition from cubic $\alpha$- to orthorhombic $\gamma$-$ZrW_2O_8$ at 0.21 GPa, and amorphization progressively from 1.5 to 3.5 GPa. High-pressure studies up to 0.6 GPa have been performed on cubic $\gamma$-$ZrMo_2O_8$.[4] However, no phase transition was reported. We report here two reversible high-pressure transitions for trigonal $\alpha$-$ZrMo_2O_8$ in a study performed up to 9.54 GPa.

Powder samples of trigonal $ZrMo_2O_8$ were prepared by dehydrating zirconium molybdenum oxide hydroxide hydrate $[ZrMo_2O_7(OH)_2(H_2O)_2]$, prepared as described by Clearfield and Blessing.[13] The crystalline starting material was heated to 450°C for 18 h in a platinum crucible and was subsequently quenched. X-ray powder pattern of the prepared sample were identical to previously published data.[8]

The x-ray-diffraction experiments were carried out at the high-pressure beamline ID30, European Synchrotron Radiation Facility (ESRF). X rays from two phased undulators were monochromatized to $\lambda = 0.42496$ Å using a channel-cut Si-crystal operated in vacuum. The x-ray beam was collimated down to $0.080 \times 0.080$ mm$^2$. A membrane driven diamond-anvil cell[14] (MDAC) equipped with 600 $\mu$m diameter diamond culets was used. Methanol-ethanol (4:1) was used as pressure transmitting medium. The samples were

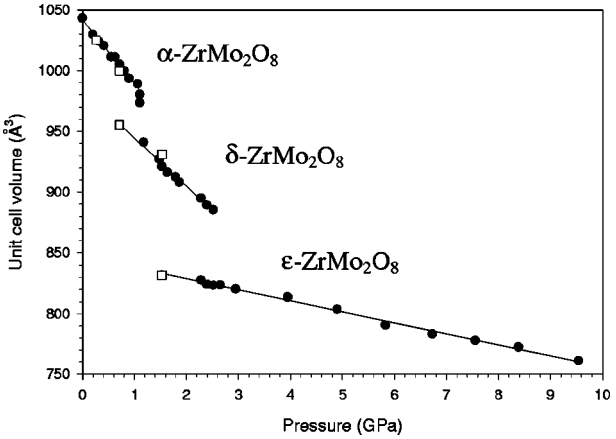


FIG. 3. The change in unit-cell volume versus pressure for $\alpha$-$ZrMo_2O_8$. The solid lines are least-squares fits to the volume data. The open squares are derived from decreasing pressure data. Unit-cell volume data for the $\delta$ and $\epsilon$ phases were multiplied by 3 for comparison with $\alpha$-$ZrMo_2O_8$.

loaded into gasket holes of 250 $\mu$m diameter together with pressure medium and a small ruby crystal. The ruby fluorescence technique[15] was used to determine the pressure.

Images of the powder diffraction rings were collected with an image-plate detector[16] (image size: 240 $\times$300 mm$^2$, pixel size: 0.07$\times$0.08 mm$^2$) placed at 450 and 500 mm from the sample. The aperture of the MDAC limits the data collection to $2\theta$ angles $\leqslant$23°. The images were corrected for spatial distortion and nonlinear features in the background, and subsequently integrated over the entire powder rings using the software FIT2D.[17]

The pressure induced changes in the diffraction pattern of $\alpha$-$ZrMo_2O_8$ are shown in Figs. 1 and 2. Already at 0.53 GPa (Fig. 1) new peaks appear at, e.g., $2\theta$=8.5, 9.5, and 13.5°. However, these peaks are compatible with the ambient pressure phase and can be indexed using the trigonal space-group symmetry $P\bar{3}c$. A major change in symmetry occurs between 1.06 and 1.11 GPa (Fig. 2), subsequently analyzed using TREOR97 (Ref. 18) and DICVOL91.[19] The pattern at 1.53 GPa in Fig. 1 was regarded as a pure phase and was used for indexing. Initial trials resulted in a number of possible orthorhombic unit cells, with a low figure of merit and unindexed lines. Only by going to monoclinic symmetry could all peaks in the patterns be indexed, resulting in the figure of merit, $M(33)=17$ (Ref. 20) and $F(33)=77$.[21] Subsequently, profile fitting (Le Bail method[22]) was performed using GSAS.[23] The reflection conditions for the indexed monoclinic high-pressure phase (hereafter $\delta$-$ZrMo_2O_8$) indicate that a possible space-group symmetry could be $C2/m$. This choice of space-group symmetry is further corroborated by preliminary structural refinements.

A second high-pressure transition occurs at 2.0–2.5 GPa (Figs. 1 and 2). After indexing the pattern at 2.95 GPa with several autoindexing programs [TREOR97,[18] DICVOL91,[19] KOHL,[24] and LZON (Ref. 25)] linked in the CRYSFIRE Suite,[26] a reasonable triclinic unit cell was found. Attempts to find a possible supercell failed, or the unit cell became unreasonably large. This phase (hereafter $\epsilon$-$ZrMo_2O_8$) show similar unit-cell dimensions to the $\delta$ phase and all lines were indexed with a resulting figure of merit, $M(20)=21$.[20] It has not been possible to distinguish between the two possible space-group symmetries, $P1$ and $P\bar{1}$. At higher pressures the peaks get broader and higher-order reflections disappear, which probably is due to the increasing nonhydrostatic conditions for the methanol-ethanol mixture above 8 GPa. Another possiblility is that the structure becomes x-ray amorphous. Higher pressure (above 8 GPa) investigations using a pressure medium with better hydrostatic characteristics ($N_2$ or Ar) are clearly needed. As can be seen from Fig. 2 the transitions are fully reversible, with a slight peak broadening remaining from the higher pressures.

TABLE II. Comparison of unit-cell axis and volume compressibilities (Ref. 27) for $ZrMo_2O_8$ and $ZrW_2O_8$. Values have the dimension $10^{-2}$GPa$^{-1}$. Below the volume compressibilities estimated bulk moduli, obtained by fitting the Birch equation of state (Ref. 28) to the volume data, are given in brackets.

| Phase | $\beta_a$ | $\beta_b$ | $\beta_c$ | $\beta_V$ |
|---|---|---|---|---|
| $\alpha$-$ZrW_2O_8$ (Ref. 12) | 0.47(1) | | | 1.38(1) |
| $\gamma$-$ZrW_2O_8$ (Ref. 12) | 0.53(1) | 0.47(1) | 0.47(1) | 1.53(1) |
| $\gamma$-$ZrMo_2O_8$ (Ref. 4) | | | | 2.24(1) |
| $\alpha$-$ZrMo_2O_8$ | 0.34(1) | | 4.26(1) | 5.07(1) |
| | | | | [17.0(3) GPa] |
| $\delta$-$ZrMo_2O_8$ | 1.50(1) | -0.32(1) | 3.08(1) | 4.24(1) |
| | | | | [19.1(3) GPa] |
| $\epsilon$-$ZrMo_2O_8$ | 0.38(1) | 0.35(1) | 0.52(1) | 1.10(1) |
| | | | | [74(1) GPa] |

The unit-cell parameters obtained from the profile fits in GSAS are listed in Table I, and the unit-cell volume changes versus pressure are shown in Fig. 3. The discontinous unit-cell-volume decrease in the transition from the $\alpha$- to $\delta$-$ZrMo_2O_8$ is 4.9%. This is comparable to the 5% volume decrease in the $\alpha$-$\gamma$ transition of $ZrW_2O_8$.[10] In Table II, the volume compressibilities[27] of $ZrMo_2O_8$ and $ZrW_2O_8$ are shown. The volume compressibility of $\alpha$-$ZrMo_2O_8$ up to the transition at 1.1 GPa is twice as high as compared to $\gamma$-$ZrMo_2O_8$, and more than three times higher than for $\alpha$-$ZrW_2O_8$. As can also be seen from Table II, the linear compressibility of the $c$ axis is, as compared to the $a$ axis, responsible for most of the volume compressibility of $\alpha$-$ZrMo_2O_8$. This can be understood by considering that the structure is built up of layers stacked in the $c$ direction. After the transition the $a$ axis of $\delta$-$ZrMo_2O_8$ displays higher compressibility, while in the $c$ direction the compressibility is comparable to the $c$ axis of $\alpha$-$ZrMo_2O_8$. However, the $b$ axis of the $\delta$ phase increases slightly with pressure (Table II). The volume compressibility of the $\delta$ phase is similar to $\alpha$-$ZrMo_2O_8$. In the transition from $\delta$- to $\epsilon$-$ZrMo_2O_8$ at 2 GPa the decrease of the unit-cell volume is 10%, and the volume compressibillity of the $\epsilon$ phase becomes 1.10 $\times10^{-2}$ GPa$^{-1}$ (Table II). Thus, the $\epsilon$ phase is considerably harder than the lower-pressure phases, as could be expected because of the higher density and closer packing of atoms. Significant hysteresis is observed for both transitions (Fig. 3 and Table I). At decreasing pressures the triclinic and monoclinic phases remain down to 1.53 and 0.71 GPa, respectively. In fact, the triclinic phase is also visible in the pattern

at 0.71 GPa, but could not be reliably indexed due to overlapping peaks from the trigonal and monoclinic phases.

In summary, fully reversible high-pressure transformations from the ambient pressure phase, $\alpha$-$ZrMo_2O_8$, to a monoclinic $\delta$ phase at 1.06–1.11 GPa, and a triclinic $\epsilon$ phase at 2.0–2.5 GPa, have been found. In view of these transitions and because of the lower density, it is highly likely that the cubic $\gamma$-$ZrMo_2O_8$ will show transformations at pressures above the previously investigated pressure range of 0–0.6 GPa.[4]


[1] T. A. Mary, J. S. O. Evans, T. Vogt, and A. W. Sleight, Science **272**, 90 (1996).

[2] J. S. O. Evans, T. A. Mary, T. Vogt, M. A. Subramanian, and A. W. Sleight, Chem. Mater. **8**, 2809 (1996).

[3] V. Korthuis, N. Khosrovani, A. W. Sleight, N. Roberts, R. Dupree, and W. W. Waren, Chem. Mater. **7**, 412 (1995).

[4] C. Lind, A. P. Wilkinson, Z. Hu, S. Short, and J. D. Jorgensen, Chem. Mater. **10**, 2335 (1998).

[5] M. Auray, C. Quarton, and P. Tarte, Acta Crystallogr., Sect. C: Cryst. Struct. Commun. **42**, 257 (1986).

[6] V. N. Serezhkin, V. A. Efremov, and V. K. Trunov, Russ. J. Inorg. Chem. **32**, 1566 (1987).

[7] R. F. Klevtsova, L. A. Glinskaya, E. S. Zolotova, and P. V. Klevtsov, Dokl. Akad. Nauk. (SSSR) **304**, 91 (1989) [Sov. Phys. Dokl. **34**, 1065 (1989)].

[8] M. Auray, M. Quarton, and P. Tarte, Powder Diffr. **2**, 36 (1987).

[9] M. Auray, M. Quarton, and P. Tarte, Powder Diffr. **4**, 29 (1989).

[10] J. S. O. Evans, Z. Hu, J. D. Jorgensen, D. N. Argyriou, S. Short, and A. W. Sleight, Science **275**, 61 (1997).

[11] C. A. Perottoni and J. A. H. Jordana, Science **280**, 886 (1998).

[12] J. D. Jorgensen, Z. Hu, S. Teslic, D. N. Argyriou, S. Short, J. S. O. Evans, and A. W. Sleight, Phys. Rev. B **59**, 215 (1999).

[13] A. Clearfield and R. H. Blessing, J. Inorg. Nucl. Chem. **34**, 2643 (1972).

[14] R. Letoullec, J. P. Pinceaux, and P. Loubeyre, High Press. Res. **1**, 77 (1988).

[15] G. J. Piermarini, S. Block, J. D. Barnett, and R. A. Forman, J. Appl. Phys. **46**, 2774 (1975).

[16] M. Thoms, S. Bachau, D. Häusermann, M. Kunz, T. Le Bihan, M. Mezouar, and D. Strawbridge, Nucl. Instrum. Methods Phys. Res. A **413**, 175 (1998).

[17] A. Hammersley, FIT2D V10.3 Reference Manual V4.0, ESRF, Grenoble, France, 1998.

[18] P.-E. Werner, L. Eriksson, and M. Westdahl, J. Appl. Crystallogr. **18**, 367 (1985).

[19] A. Boultif and D. Louër, J. Appl. Crystallogr. **24**, 987 (1991).

[20] P. M. De Wolff, J. Appl. Crystallogr. **5**, 108 (1968).

[21] G. S. Smith and R. L. Snyder, J. Appl. Crystallogr. **12**, 60 (1979).

[22] A. Le Bail, H. Duroy, and J. L. Fourquet, Mater. Res. Bull. **23**, 447 (1988).

[23] A. C. Larson and R. B. Von Dreele, LANSCE MS-H805, Los Alamos National Laboratory, Los Alamos, NM, 1994.

[24] F. Kohlbeck and E. M. Hörl, J. Appl. Crystallogr. **11**, 60 (1978).

[25] R. Shirley and D. Louër, Acta Crystallogr., Sect. A: Cryst. Phys., Diffr., Theor. Gen. Crystallogr. **34**, S382 (1978).

[26] R. Shirley, The CRYSFIRE System for Automatic Powder Indexing: User's Manual, The Lattice Press, 41 Guildford Park Avenue, Guildford, Surrey, GU2 5NL, England, 1999.

[27] The compressibility is defined as $\beta_x = -(1/x)(\Delta x/\Delta P)$, where $x$ is the unit-cell volume or axis length.

[28] F. Birch, J. Geophys. Res. **57**, 227 (1952). The Birch equation of state is defined as $P=(3/2)B_0[(V/V_0)^{-7/3}-(V/V_0)^{-5/3}]$, where $B_0$ is the bulk modulus at zero pressure.